METABOLIC MODELING OF CONVERGING METABOLIC PATHWAYS

Analysis of Non-steady State Stable Isotope-resolve Metabolism of UDP-GlcNAc and UDP-GalNAc

Hunter N. B. Moseley, Richard M. Higashi, Teresa W-M. Fan

Department of Chemistry, University of Louisville, 2320 S Brook Street, Louisville, KY 40292, U.S.A.
Structural Biology Program, JG Brown Cancer Center, University of Louisville, Louisville, KY 40202, U.S.A.
{hunter.moseley, rick.higashi}@louisville.edu, twmfan@gmail.com

Andrew N. Lane

Department of Chemistry, University of Louisville, 2320 S Brook Street, Louisville, KY 40292, U.S.A.
Structural Biology Program, JG Brown Cancer Center, University of Louisville, Louisville, KY 40202, U.S.A.
Department of Medicine, Clinical Translational Research Building, 505 S. Hancock St., Louisville KY 40202, U.S.A.
andrew.lane@louisville.edu

Abstract: We have developed a novel metabolic modeling methodology that traces the flow of functional moieties (chemical substructures) through metabolic pathways via the deconvolution of mass isotopologue data of specific metabolites. We have implemented a general simulated annealing/genetic algorithm for parameter optimization called Genetic Algorithm for Isotopologues in Metabolic Systems (GAIMS), with a model selection method developed from the Akaike information criterion. GAIMS is tailored for analysis of ultra-high resolution, high mass-accuracy isotopologue data from Fourier transform-ion cyclotron resonance mass spectrometry (FT-ICR-MS) for interpretation of non-steady state stable isotope-resolved metabolomics (SIRM) experiments. We applied GAIMS to a time-course of uridine diphospho-N-acetylglucosamine (UDP-GlcNAc) and uridine diphospho-N-acetylgalactosamine (UDP-GalNAc) isotopologue data obtained from LNCaP-LN3 prostate cancer cells grown in [U-^{13}C]-glucose. The best metabolic model was identified, which revealed the relative contribution of specific metabolic pathways to ^{13}C incorporation from glucose into individual functional moieties of UDP-GlcNAc and UDP-GalNAc. Furthermore, this analysis allows direct comparison of MS isotopologue data with NMR positional isotopomer data for independent experimental cross-verification.

1 INTRODUCTION

Modeling of cellular metabolism is a well-established technique for studying the flow of matter and energy through cells for a variety of purposes including: i) understanding cellular growth (Edwards et al., 2001), ii) determining the effects of gene and signalling pathways on cellular metabolism (Sauer, 1999); and iii) detection of biomarkers (Harrigan and Goodacre, 2003). Several common and related modeling techniques such as metabolic balance analysis (Fell, 1984; Savinell and Palsson, 1992; Kaufman et al., 2003) and metabolic control analysis

(Fell, 1997; Stephanopoulos, 1999; Hellerstein, 2003; Sauer, 2006) have been developed which use a series of differential equations to model the flux of metabolites. These techniques typically require steady-state conditions that allow the application of standard numerical methods to solve a system of differential equations in the form of an eigensystem. While steady-state conditions are often assumed, in reality they are quite hard to establish, maintain, and verify for actual experiments involving mammalian cells. For multicellular organisms, steady state conditions for all metabolites are practically impossible to establish. Also, most applications of
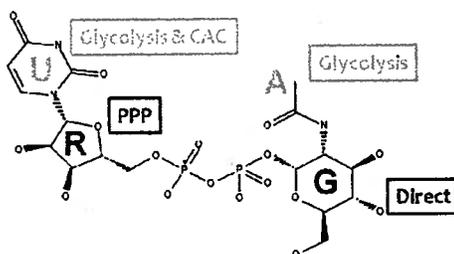
Figure 1: Structure of UDP-GlcNAc labeled by its functional moieties and their biosynthetic pathways from a [U- ^{13}C]-glucose source. Uracil moiety is derived from glycolysis, citric acid cycle and pyrimidine biosynthesis. Ribose moiety is derived from the pentose phosphate pathway and pyrimidine biosynthesis. Acetyl moiety is derived from glycolysis. Glucose moiety is directly incorporated. UDP-GalNAc has an identical structure and pathway derivation with glucose replaced by its isomer Galactose.
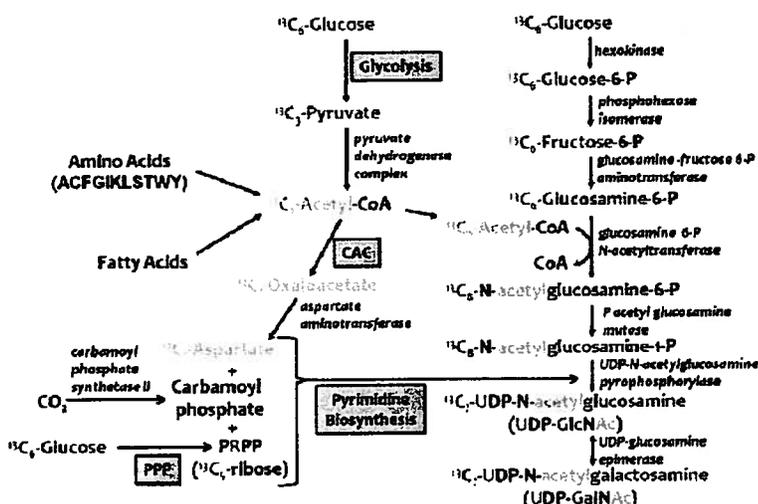

Figure 2: Converging metabolic pathways leading from [U-^{13}C]-glucose to UDP-GlcNAc and UDP-GalNAc. ^{13}C-labeled glucose is incorporated into the nucleotide sugars via four routes: i) direct incorporation via the right UDP-hexose biosynthetic pathway; ii) via glycolysis; iii) via glycolysis, citric acid acid cycle, and pyrimidine biosynthesis; and iv) via the pentose phosphate pathway and pyrimidine biosynthesis.

these modelling techniques rely on total metabolite concentrations or isotopic ratios derived from experiment, which creates an underdetermined system of equations where there are more variables than independent data. Thus, unique meaningful solutions to these numerical systems are not always possible (Schellenberger and Palsson, 2009) and their use in testing model validity is therefore limited.

Using stable isotope resolved metabolomics (SIRM) to determine individual isotopomers and isotopologues detected by NMR and mass spectrometry, respectively, can greatly increase the ratio of experimental data to equation variables (Lane et al., 2009). Supplying [U-^{13}C]-glucose to cells in culture allows each carbon in a detected metabolite to be a separate sensor for ^{13}C incorporation. However, detection, resolution, and

unique identification of individual isotopologues requires the ultra-high mass accuracy provided by FT-ICR-MS (Lane et al., 2008; Lane et al., 2009; Moseley, 2010). Moreover, steady-state conditions are even harder to establish with isotopomer and isotopologue data (Lane et al., 2009), and may be undesirable when one seeks to maximize the information content of the data (Wahl et al., 2008).

Since steady-state conditions for SIRM experiments are neither achievable, nor desirable in mammalian cells, we have developed a novel metabolic modeling methodology that interprets isotopologue data of detected metabolites as flows of functional moieties through metabolic pathways.

Such moieties correspond to actual, individual biochemical entities, rather than sums of species. These moiety models are optimized using a combined simulated annealing genetic algorithm

109

called Genetic Algorithm for Isotopologues in Metabolic Systems (GAIMS). GAIMS optimizes model variables to fit a given moiety model to isotopologue data of specific metabolites obtained from non-steady state SIRM experiments.

We used GAIMS to optimize moiety models against time-course isotopologue data for UDP-GlcNAc and UDP-GalNAc obtained from LNCaP-LN3 prostate cancer cells grown in [U- ^{13}C]-glucose. Metabolic control of UDP-GlcNAc and UDP-GalNAc underlies the regulation of many biological processes via O-linked glycosylation of proteins, including nutrient sensing, protein degradation, gene expression (Hart et al., 2007), and embryogenesis (Gambetta et al., 2009). UDP-GlcNAc and UDP-GalNAc are composed of four functional moieties as shown in Figure 1: glucose or galactose, ribose, acetyl, and UDP. These four functional moieties represent the convergence of several major metabolic pathways that lead from [U- ^{13}C]-glucose to UDP-GlcNAc and UDP-GalNAc biosynthesis as shown in Figure 2. These pathways include glycolysis, the citric acid cycle, the pentose phosphate pathway, pyrimidine biosynthesis, and the UDP-hexose biosynthetic pathway referred to as the "direct" pathway. Furthermore, other carbon sources can contribute to the synthesis of the uracil and acetyl moieties, to an extent that is cell and condition dependent. The moiety modeling seeks to determine the relative contributions for each pathway segment.

UDP-GlcNAc and UDP-GalNAc are handled together in this analysis because as these two metabolites have identical mass-to-charge ratios, the isotopologue peak intensities are the sum of both metabolites. However, from NMR isotopomer analysis (data not shown), UDP-GlcNAc is the major contributor to the isotopologue intensities and that this contribution is proportional across the set of isotopologue peaks. This makes logical sense because UDP-GlcNAc and UDP-GalNAc are separated by a single reversible enzymatic reaction catalyzed by the UDP-glucosamine epimerase.

2 METHODS

2.1 Data Acquisition and Natural Abundance Correction

LNCaP-LN3 prostate cancer cells (donated from Roswell Park) were grown to 70% confluence at 37° C in RPMI 1640 medium supplemented with: 10% FBS, 100 units/mL penicillin, 100 µg/mL

streptomycin, 0.2% glucose, and 5% CO_2. Next, medium was replaced with a similar RPMI 1640 medium containing 0.2% [U-^{13}C] glucose. Cells were harvested at different time points, centrifuged, extracted with 10% trichloroacetic acid, lyophilized, and dissolved in H_2O. These samples were then analyzed via direct infusion nanoelectrospray FT-ICR-MS in negative ion mode using a Thermo 7T LTQ FT-MS. Isotopologue peaks were assigned using the software PREMISE (Lane et al., 2009) and each peak intensity was measured and normalized to the sum of the isotopologue intensities:

$$I_{n,obs} = I_{n,raw}/\Sigma\ I_{i,raw} \qquad (1)$$

Finally, the set of UDP-GlcNAc and UDP-GalNAc isotopologue intensities were corrected for ^{13}C natural abundance using the following three equations implemented in an iterative algorithm (Moseley, 2010).

$$B_C(n,k) = \binom{C_{Max}-n}{k-n}(1-NA_{13_C})^{C_{Max}-k}NA_{13_C}^{k-n} \qquad (2)$$

$$B_C sum(n) = \sum_{k=n+1}^{C_{Max}} B_C(n,k) \qquad (3)$$

$$I_{M+i} = \frac{I_{M+i;NA} - \sum_{x=0}^{x<i} I_{M+x} * B_C(x,i)}{1 - B_C sum(i)} \qquad (4)$$

2.2 Moiety Modeling

As is shown in Figure 1, UDP-GlcNAc is composed of four functional moieties, glucose, ribose, acetyl, and uracil, representing convergence of several metabolic pathways. We can represent each moiety as a set of state variables reflecting the probabilities of ^{13}C incorporation into each moiety. The state variables g0,r0,a0,u0 represent the probability of no ^{13}C incorporation in glucose, ribose, acetyl, and uracil, respectively. From Figure 2, it seems reasonable to restrict ^{13}C incorporation for glucose, ribose, and acetyl to the fully labelled state variables g6, r5, and a2, respectively. This is experimentally corroborated by the absence of partially labelled isotopomers of glucose, ribose, and acetate. Naturally, then the following relationships hold for the state variables of glucose, ribose, and acetyl:

$$\begin{aligned} g6 &= 1 - g0 \\ r5 &= 1 - r0 \\ a2 &= 1 - a0 \end{aligned} \qquad (5)$$

However, the biosynthesis of uracil mixes ^{13}C from labelled glucose via ^{13}C$_2$-acetyl-CoA with ^{12}C from other (unlabeled) sources during the citric acid

cycle. Thus, multiple state variables , , and must be used to represent the partial labelling of uracil. There is no state variable since one carbon of uracil is derived from unlabeled CO_2. These state variables have the following relationship:

$$u0 + \; + \; + \; = 1 \qquad (6)$$

The state variables for all four moieties can describe the probabilities for 32 different isotopomers of UDP-GlcNAc and the intensities for 18 isotopologues via the following set of equations:

$$I_0 = g0r0a0u0$$
$$I_1 = g0r0a0$$
$$I_2 = g0r0a0 \;\; + g0r0 \;\; u0$$
$$I_3 = g0r0a0 \;\; + g0r0$$
$$I_4 = g0r0$$
$$I_5 = g0r5a0u0 + g0r0$$
$$I_6 = g6r0a0u0 + g0r5a0$$
$$I_7 = g6r0a0 \;\; + g0r5 \;\; u0 + g0r5a0$$
$$I_8 = g6r0 \;\; u0 + g6r0a0 \;\; + g0r5a0 \;\; + g0r5$$
$$I_9 = g6r0a0 \;\; + g6r0 \;\; + g0r5 \qquad (7)$$
$$I_{10} = g6r0 \;\; + g0r5$$
$$I_{11} = g6r5a0u0 + g6r0$$
$$I_{12} = g6r5a0$$
$$I_{13} = g6r5a0 \;\; + g6r5 \;\; u0$$
$$I_{14} = g6r5a0 \;\; + g6r5$$
$$I_{15} = g6r5$$
$$I_{16} = g6r5$$
$$I_{17} = NA \; contribution \; only$$

In addition, these state variables and their constraining relationships provide six optimizable parameters ($g6$, $r5$, , , ,), one each for glucose, ribose, and acetyl and three for uracil. These variables are time dependent, and constitute the starting point for detailed flux analysis of the specific metabolic network that described the synthesis of the observed product.

2.3 GAIMS

To extract the variables from the data, we have developed a combined simulated annealing and genetic algorithm called Genetic Algorithm for Isotopologues in Metabolic Systems (GAIMS) to optimize moiety model parameters. GAIMS uses a description of the moiety model to calculate isotopologue intensities (Equations 7). The program then uses these calculated isotopologue intensities ($I_{n,calc}$) with the observed experimental isotopologue intensities ($I_{n,obs}$) to create a target function that compares calculated isotopologue intensities to their experimentally observed counterparts:

$$target\_function = \Sigma abs(I_{n,obs} - I_{n,calc}) \qquad (8)$$

Other target functions were tested including the commonly used sum of squared differences; however, that function tended to fit stronger isotopologue intensities at the expense of weaker isotopologue intensities. Also, target functions normalized by intensity demonstrated poorer convergence, probably due to the higher fractional error in the weaker isotopologue intensities. Overall, the target function represented by Equation 8 provided the best behaviour.

For each parameter optimization, GAIMS used a linear annealing scheme over 1,000,000 steps. Genetic algorithm settings included a population size of 20 with a cross-over versus mutation rate ratio of 1:20. Mutation steps changed three parameters at a time to compensate for any dependencies between parameters. Each optimization was performed 50 times to verify robustness (i.e. avoidance of local minima) and to provide meaningful statistics of convergence.

2.4 Model Selection using AIC

We developed a model selection method using the following form of the Akaike information criterion or AIC (Akaike, 1974):

$$AIC \approx 2k + n \log\left(\frac{\sum_{i=1}^{n}(I_{i,obs} - I_{i,calc})^2}{n}\right) \qquad (9)$$

In Equation 9, k is the number of moiety model parameters being optimized. The log of the average sum of squares of differences approximates the log likelihood of a given model. The calculated isotopologue intensities $I_{i,calc}$ are derived from average moiety model parameters for all 50 optimizations. With this equation, we can compare models with a different number of optimizable parameters. This model selection method was developed as a part of GAIMS.

3 RESULTS

3.1 Fit of Expert-derived Moiety Model

Figure 3 shows the fit of calculated isotopologue intensities from the expert-derived moiety model (Equations 7) to the 72-hour time point of experimental isotopologue intensities representing

both UDP-GlcNAc and UDP-GalNAc. From this fit, we obtain values for each functional moiety state variable. All fifty optimizations converged quite well as indicated by the standard deviations in state variables. Interestingly, the fit of high intensity isotopologues appears better than low intensity isotopologues. In addition, we repeated this analysis with 50 optimizations using 10,000,000 steps and 50 optimizations using 100,000 steps and obtained very similar results in both parameter values and standard deviations (data not shown), further demonstrating the robustness of the parameter optimization.
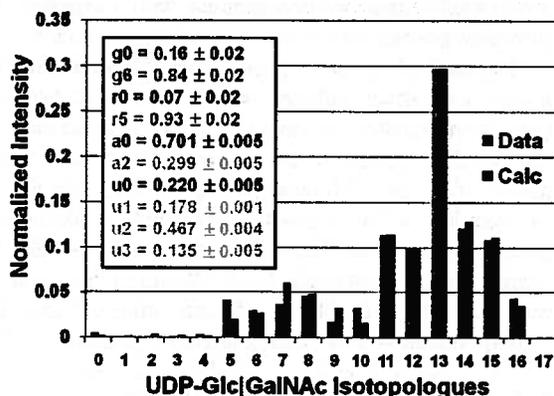

Figure 3: Fit of optimized expert-derived moiety model to FT-ICR-MS isotopologue data of UDP-GlcNAc and UDP-GalNAc from tissue culture sample after 72 hours of labeling with uniformly ^{13}C-labeled glucose.

3.2 Comparison of Models using a Target Function

To explore reasons why some of the low intensity isotopologues did not fit as well, we examined alternative moiety models that tested assumptions of our original model. From the pathway diagram in Figure 2, there is the possibility that scrambling of ^{13}C incorporation in the acetyl moiety might be occurring via amino acid biosynthetic and catabolic pathways on the time-scale of 72 hours. So we created an extended acetyl model with additional terms (i.e., $I_1 = g0r0a0u1 + g0r0a1u0$) in Equations 7 using the acetyl moiety state variable a1 along with the following relationship:

$$a0 + a1 + a2 = 1 \qquad (10)$$

In a similar manner, we created another alternative moiety model with the addition of the u4 state variable for the uracil moiety. This CO_2-inclusive model tested the hypothesis that all CO_2 used in uracil biosynthesis is unlabeled. Likewise,

the relationship between uracil state variables was expanded in the following manner:

$$u0 + u1 + u2 + u3 + u4 = 1 \qquad (11)$$

Table 1 shows the comparison between the three moiety models. The value indicated for the target function is the average across all 50 optimizations for each model. Equation 8 clearly indicates that this is a minimizing target function and thus lower values are better.

Table 1: Comparison between three moiety models using the average value of the target function.

CO$_2$-Inclusive (7_G1R1A1U4)	Expert-Derived (6_G1R1A1U3)	Extended Acetyl (7_G1R1A2U3)
TF = 0.1103	TF = 0.1096	TF = 0.0913
g0 = 0.15	g0 = 0.16	g0 = 0.15
g6 = 0.85	g6 = 0.84	g6 = 0.85
r0 = 0.08	r0 = 0.07	r0 = 0.08
r5 = 0.92	r5 = 0.93	r5 = 0.92
a0 = 0.70	a0 = 0.70	a0 = 0.28
a2 = 0.30	a2 = 0.30	a1 = 0.15
u0 = 0.22	u0 = 0.22	a2 = 0.57
u1 = 0.18	u1 = 0.18	u0 = 0.54
u2 = 0.47	u2 = 0.47	u1 = 0.15
u3 = 0.14	u3 = 0.14	u2 = 0.22
u4 = 0.001		u3 = 0.09

The results in Table 1 clearly indicate that the CO_2-inclusive model is worse than the expert-derived model. Moreover, the extended acetyl model appears to be the best model. However, the extended acetyl model has one additional optimizable parameter, which might afford the improvements observed in the target function.

We also optimized an additional CO_2-inclusive model where the ^{13}C incorporation via CO_2 was modelled as its own state variables c0 and c1. This moiety model gave very similar results to those for the original CO_2-inclusive model, indicating that the specific implementation of a model is not critical (data not shown).

3.3 Comparison of Models using AIC

We used the form of the AIC in Equation 9 to address the issue of model comparison involving different number of optimizable parameters. The AIC is calculated for each model using the average parameter values across the 50 GAIMS optimizations. But instead of just comparing three possible models, we created a set of over 40 moiety models to compare, ranging from plausible to completely nonsense models. The expert-derived model is represented by the identifier 6_G1R1A1U3, where the first number indicates the number of optimizable parameters in the model and

G1R1A1U3 represents one parameter in the glucose moiety, one parameter in the ribose moiety, one parameter in the acetyl moiety, and three parameters in the uracil moiety, respectively. Deviations from the expert-derived model are indicated by state variables that are modified or added.

Table 2: Comparison of 40 moiety models using the AIC and the experimental FT-ICR-MS isotopologue data of UDP-GlcNAc and UDP-GalNAc at the 72-hour time point.

AIC	Moiety Model
-157.43	6_G0R2A1U3_g3r2r3_g6r5
-109.64	6_G1R1A1U3_a1
-136.29	6_G1R1A1U3_g5
-154.32	6_G1R1A1U3
-137.17	6_G1R1A1U3_r4
-133.12	6_G1R1A1U3_u4
-159.00	7_G0R2A2U3_g3r2r3_g6r5
-72.52	7_G0R3A1U3_g3r2r3_g6r5_g5r4
-72.52	7_G0R3A1U3_g3r2r3_g6r5_r4
-151.40	7_G1R1A1U3C1
-153.52	7_G1R1A1U4
-156.29	7_G1R1A2U3
-158.25	7_G1R2A1U3_g3r2r3
-153.65	7_G1R2A1U3_r1
-159.24	7_G1R2A1U3_r2
-147.55	7_G1R2A1U3_r3
-163.39	7_G1R2A1U3_r4
-153.95	7_G2R1A1U3_g1
-153.64	7_G2R1A1U3_g2
-158.87	7_G2R1A1U3_g3
-151.21	7_G2R1A1U3_g4
-160.84	7_G2R1A1U3_g5
-154.17	8_G1R1A2U3C1
-156.58	8_G1R2A2U3_g3r2r3_g6r5_g5
-158.22	8_G1R2A2U3_g3r2r3
-154.14	8_G1R2A2U3_r1
-159.10	8_G1R2A2U3_r2
-157.39	8_G1R2A2U3_r2r3
-148.47	8_G1R2A2U3_r3
-161.97	8_G1R2A2U3_r4
-153.91	8_G2R1A2U3_g1
-154.09	8_G2R1A2U3_g2
-158.85	8_G2R1A2U3_g3
-151.36	8_G2R1A2U3_g4
-159.52	8_G2R1A2U3_g5
-155.89	9_G2R2A2U3_r2r3_g1
-154.77	9_G2R2A2U3_r2r3_g2
-156.24	9_G2R2A2U3_r2r3_g3
-152.79	9_G2R2A2U3_r2r3_g4
-156.13	9_G2R2A2U3_r2r3_g5
-155.50	9_G2R2A2U3_r2r3_g6r5_g3_g5

Table 2 shows the AIC for all these models based on the 72-hour time point of experimental isotopologue intensities. The models in red all indicate AICs that are better than the expert-derived model. However, the 7_G1R2A1U3_r4 model gave

the best (lowest) AIC even though this model with ribose state variables r5, r4, and r0 makes no biochemical sense given the known information about the pentose phosphate pathway in human cells. In fact, many nonsense models gave better results than the expert-derived model, indicating a significant problem with overfitting.

3.4 Model Selection using AIC with Multiple Time Points

Table 3: Comparison of 40 moiety models using the AIC and the experimental FT-ICR-MS isotopologue data of UDP-GlcNAc and UDP-GalNAc at the 34-hour, 48-hour, and 72-hour time points.

AIC	Moiety Model
-321.81	6_G0R2A1U3_g3r2r3_g6r5
-355.87	6_G1R1A1U3_a1
-326.98	6_G1R1A1U3_g5
-428.98	6_G1R1A1U3
-332.69	6_G1R1A1U3_r4
-308.16	6_G1R1A1U3_u4
-291.31	7_G0R2A2U3_g3r2r3_g6r5
-287.32	7_G0R3A1U3_g3r2r3_g6r5_g5r4
-290.16	7_G0R3A1U3_g3r2r3_g6r5_r4
-306.58	7_G1R1A1U3C1
-293.12	7_G1R1A1U4
-299.86	7_G1R1A2U3
-294.52	7_G1R2A1U3_g3r2r3
-308.59	7_G1R2A1U3_r1
-288.94	7_G1R2A1U3_r2
-277.44	7_G1R2A1U3_r3
-244.47	7_G1R2A1U3_r4
-318.01	7_G2R1A1U3_g1
-317.89	7_G2R1A1U3_g2
-286.93	7_G2R1A1U3_g3
-277.12	7_G2R1A1U3_g4
-252.21	7_G2R1A1U3_g5
-288.84	8_G1R1A2U3C1
-296.01	8_G1R2A2U3_g3r2r3_g6r5_g5
-288.88	8_G1R2A2U3_g3r2r3
-290.93	8_G1R2A2U3_r1
-296.67	8_G1R2A2U3_r2
-296.18	8_G1R2A2U3_r2r3
-251.87	8_G1R2A2U3_r3
-239.25	8_G1R2A2U3_r4
-303.97	8_G2R1A2U3_g1
-293.45	8_G2R1A2U3_g2
-288.32	8_G2R1A2U3_g3
-260.59	8_G2R1A2U3_g4
-236.42	8_G2R1A2U3_g5
-293.74	9_G2R2A2U3_r2r3_g1
-279.33	9_G2R2A2U3_r2r3_g2
-291.46	9_G2R2A2U3_r2r3_g3
-241.63	9_G2R2A2U3_r2r3_g4
-227.58	9_G2R2A2U3_r2r3_g5
-276.84	9_G2R2A2U3_r2r3_g6r5_g3_g5

To address the issue of overfitting, we optimized the isotopologue data for the 34-hour, 48-hour, and 72-hour time points simultaneously and calculated an AIC for the combined optimization. The expert-derived model had the best AIC of -428.98. The next best model 6_G1R1A1U3_a1 was significantly worse with an AIC of -355.87, indicating that overall, the expert-derived model provides the best description of the data.

4 CONCLUSIONS

We have demonstrated a novel metabolic modelling methodology applied to FT-ICR-MS isotopologue intensity data for UDP-GlcNAc and UDP-GalNAc. Our implementation, GAIMS, interprets a set of isotopologues as the flow of functional moieties through metabolic pathways. This is represented by a set of optimizable parameters for a given moiety model. Figure 2 demonstrates a solid convergence of 50 individual optimizations for an expert-derived model based on what is currently known about UDP-GlcNAc biosynthesis. However, the standard deviations for parameter values should not be interpreted as a close representation of parameter error, especially with the indication of model overfitting in results from Table 2.

In addition, we demonstrate a robust model selection method, which uses a form of the Akaike information criterion (Equation 9). Our use of the average parameter values from a set of optimizations allows the AIC to sense smoothness of the error surface for the target function of a given moiety model. This application of the AIC along with the use of isotopologues from multiple time points enables our model selection method to overcome issues of model overfitting for a set of isotopologues at individual time points. We envision the coupling of this robust model selection method with newer non-steady-state metabolic flux analytical methods (Selivanov et al., 2006; Wahl et al., 2008) as a logical next step.

ACKNOWLEDGEMENTS

REFERENCES

Akaike, H., 1974. "A new look at the statistical model identification", *IEEE Transactions on Automatic Control*, 19, 716–723.

Edwards, J. S., Ibarra, R. U., Palsson, B. O., 2001. "In silico predictions of *Escherichia coli* metabolic capabilities are consistent with experimental data", *Nature Biotech*, 19, 125-130.

Fell, D. A., 1984. "Fat synthesis in adipose tissue. An examination of stoichiometric constraints", *J Biochem*, 238, 781-786.

Fell, D.A., 1997. *Understanding the Control of Metabolism*, London: Portland Press.

Gambetta, M. C., Oktaba, K., & Müller, J., 2009. "Essential Role of the Glycosyltransferase Sxc/Ogt in Polycomb Repression", *Science*, 325, 93-96.

Harrigan, G. G., Goodacre, R. (Ed), 2003. *Metabolic profiling: its role in biomarker discovery and gene function analysis*, Boston: Kluwer Academic Publishers.

Hart G. W., Housley M. P., Slawson C., 2007. "Cycling of O-linked beta-N-acetylglucosamine on nucleocytoplasmic proteins", *Nature*, 446, 1017-1022.

Hellerstein, M. K., 2003. "In vivo measurement of fluxes through metabolic pathways: the missing link in functional genomics and pharmaceutical research", *Annu Rev Nutr*, 23, 379-402.

Kauffman, K. J., Prakash, P., Edwards, J. S., 2003. "Advances in flux balance analysis", *Curr Opin Biotech*, 14, 491-496.

Lane A. N., Fan T. W-M., Higashi R. M., 2008. "Isotopomer-based metabolomic analysis by NMR and mass spectrometry". *Methods in Cell Biology*, Vol 84. Biophysical Tools for Biologists, Vol 1, ed. Correia JJ, Detrich HW. Elsevier Science & Technology Books Ch.18. 541-588.

Lane, A. N., Fan, T. W-M., Xie, Z., Moseley, H. N. B., Higashi, R. M., 2009. "Stable isotope analysis of lipid biosynthesis by high resolution mass spectrometry and NMR.", *Anal Chim Acta*, 651, 201-208.

Moseley, H. N. B., 2010. "Correcting for the Effects of Natural Abundance in Stable Isotope Resolved Metabolomics Experiments Involving Ultra-High Resolution Mass Spectrometry", *BMC Bioinformatics*, 11, 139-144.

Savinell, J. M., Palsson, B. O., "Optimal selection of metabolic fluxes for in vivo measurement. I. Development of mathematical methods", *J Theor Biol*, 155, 201-214.

Sauer, U., Lasko, D. R., Fiaux, J., Hochuli, M., Glaser, R., Szyperski, T., Wuthrich, K., Bailey, J. E., 1999. "Metabolic Flux Ratio Analysis of Genetic and Environmental Modulations of Escherichia coli

Central Carbon Metabolism", *J Bacteriol*, 181, 6679-6688.

Sauer, U., 2006. "Metabolic networks in motion: 13C-based flux analysis", *Mol Syst Biol*, 2, 62.

Schellenberger, J., Palsson, B. O., 2009. "Use of Randomized Sampling for Analysis of Metabolic Networks", *J Biol Chem*, 284, 5457-5461.

Selivanov, V. A., Marin, S., Lee, P. W. N., Cascante, M., 2006. "Software for dynamic analysis of tracer-based metabolomics data: estimation of metabolic fluxes and their statistical analysis", *Bioinformatics*, 22, 2806-2812.

Stephanopoulos, G., "Metabolic fluxes and metabolic engineering", *Metab Eng*, 1, 1-11.

Wahl, S. A., Nöh, K., Wiechert, W., 2008. "13C labelling experiments at metabolic nonstationary conditions: An exploratory study", *BMC Bioinformatics*, 9, 152-169.

METABOLIC MODELING OF CONVERGING METABOLIC PATHWAYS
Analysis of Non-Steady State Stable Isotope-Resolve Metabolism of UDP-GlcNAc and UDP-GalNAc

Hunter N.B. Moseley, Richard M. Higashi, Teresa W-M. Fan,
Department of Chemistry, University of Louisville, 2320 S Brook Street, Louisville, KY 40292 USA
Structural Biology Program, JG Brown Cancer Center, University of Louisville, Louisville, KY 40202 USA
hunter.moseley@louisville.edu, rick.higashi@louisville.edu, twmfan@gmail.com

Andrew N. Lane
Department of Chemistry, University of Louisville, 2320 S Brook Street, Louisville, KY 40292 USA
Structural Biology Program, JG Brown Cancer Center, University of Louisville, Louisville, KY 40202 USA
Department of Medicine, Clinical Translational Research Building, 505 S. Hancock St., Louisville KY 40202 USA
andrew.lane@louisville.edu

Abstract: We have developed a novel metabolic modeling methodology that traces the flow of functional moieties (chemical substructures) through metabolic pathways via the deconvolution of mass isotopologue data of specific metabolites. We have implemented a general simulated annealing/genetic algorithm for parameter optimization called Genetic Algorithm for Isotopologues in Metabolic Systems (GAIMS), with a model selection method developed from the Akaike information criterion. GAIMS is tailored for analysis of ultra-high resolution, high mass-accuracy isotopologue data from Fourier transform-ion cyclotron resonance mass spectrometry (FT-ICR-MS) for interpretation of non-steady state stable isotope-resolved metabolomics (SIRM) experiments. We applied GAIMS to a time-course of uridine diphospho-N-acetylglucosamine (UDP-GlcNAc) and uridine diphospho-N-acetylgalactosamine (UDP-GalNAc) isotopologue data obtained from LNCaP-LN3 prostate cancer cells grown in [U-^{13}C]-glucose. The best metabolic model was identified, which revealed the relative contribution of specific metabolic pathways to ^{13}C incorporation from glucose into individual functional moieties of UDP-GlcNAc and UDP-GalNAc. Furthermore, this analysis allows direct comparison of MS isotopologue data with NMR positional isotopomer data for independent experimental cross-verification.

1 INTRODUCTION

Modeling of cellular metabolism is a well-established technique for studying the flow of matter and energy through cells for a variety of purposes including: i) understanding cellular growth (Edwards et al., 2001), ii) determining the effects of gene and signalling pathways on cellular metabolism (Sauer, 1999); and iii) detection of biomarkers (Harrigan and Goodacre, 2003). Several common and related modeling techniques such as metabolic balance analysis (Fell, 1984; Savinell and Palsson, 1992; Kaufman et al., 2003) and metabolic control analysis (Fell, 1997; Stephanopoulos, 1999; Hellerstein, 2003; Sauer, 2006) have been developed which use a series of differential equations to model the flux of metabolites. These techniques typically require steady-state conditions that allow the application of standard numerical methods to solve a system of differential equations in the form of an eigensystem. While steady-state conditions are often assumed, in reality they are quite hard to establish, maintain, and verify for actual experiments involving mammalian cells. For multicellular organisms, steady state conditions for all metabolites are practically impossible to establish. Also, most applications of these modelling techniques rely on total metabolite concentrations or isotopic ratios derived from

experiment, which creates an underdetermined system of equations where there are more variables than independent data. Thus, unique meaningful solutions to these numerical systems are not always possible (Schellenberger and Palsson, 2009) and their use in testing model validity is therefore limited.

Using stable isotope resolved metabolomics (SIRM) to determine individual isotopomers and isotopologues detected by NMR and mass spectrometry, respectively, can greatly increase the ratio of experimental data to equation variables (Lane et al., 2009). Supplying [U-^{13}C]-glucose to cells in culture allows each carbon in a detected metabolite to be a separate sensor for ^{13}C incorporation. However, detection, resolution, and unique identification of individual isotopologues requires the ultra-high mass accuracy provided by FT-ICR-MS (Lane et al., 2008; Lane et al., 2009; Moseley, 2010). Moreover, steady-state conditions are even harder to establish with isotopomer and isotopologue data (Lane et al., 2009), and may be undesirable when one seeks to maximize the information content of the data (Wahl et al., 2008).

Since steady-state conditions for SIRM experiments are neither achievable, nor desirable in mammalian cells, we have developed a novel metabolic modeling methodology that interprets isotopologue data of detected metabolites as flows of functional moieties through metabolic pathways.
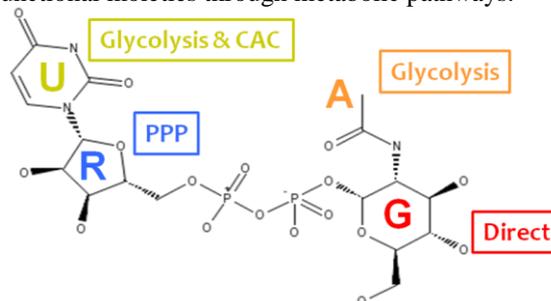

Figure 1: Structure of UDP-GlcNAc labeled by its functional moieties and their biosynthetic pathways from a [U-^{13}C]-glucose source. Uracil moiety is derived from glycolysis, citric acid cycle and pyrimidine biosynthesis. Ribose moiety is derived from the pentose phosphate pathway and pyrimidine biosynthesis. Acetyl moiety is derived from glycolysis. Glucose moiety is directly incorporated. UDP-GalNAc has an identical structure and pathway derivation with glucose replaced by its isomer Galactose.
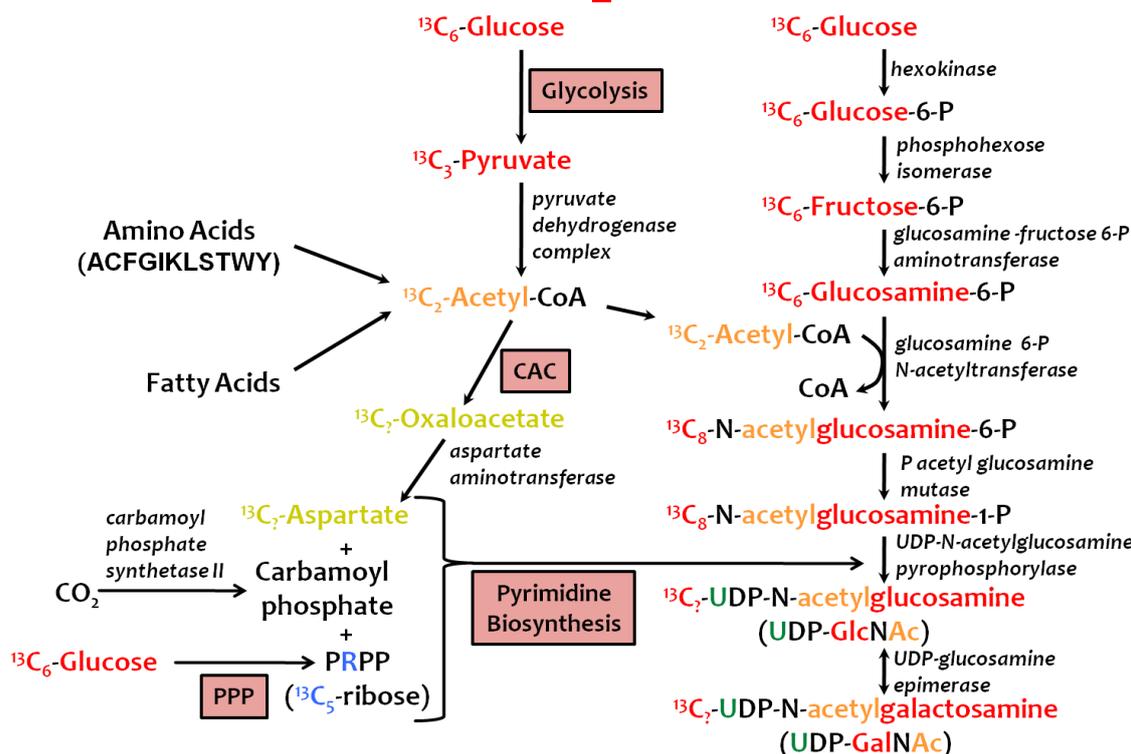

Figure 2: Converging metabolic pathways leading from [U-^{13}C]-glucose to UDP-GlcNAc and UDP-GalNAc. ^{13}C-labeled glucose is incorporated into the nucleotide sugars via four routes: i) direct incorporation via the right UDP-hexose biosynthetic pathway; ii) via glycolysis; iii) via glycolysis, citric acid acid cycle, and pyrimidine biosynthesis; and iv) via the pentose phosphate pathway and pyrimidine biosynthesis.

Such moieties correspond to actual, individual biochemical entities, rather than sums of species. These moiety models are optimized using a combined simulated annealing genetic algorithm called Genetic Algorithm for Isotopologues in Metabolic Systems (GAIMS). GAIMS optimizes model variables to fit a given moiety model to isotopologue data of specific metabolites obtained from non-steady state SIRM experiments.

We used GAIMS to optimize moiety models against time-course isotopologue data for UDP-GlcNAc and UDP-GalNAc obtained from LNCaP-LN3 prostate cancer cells grown in [U- ^{13}C]-glucose. Metabolic control of UDP-GlcNAc and UDP-GalNAc underlies the regulation of many biological processes via O-linked glycosylation of proteins, including nutrient sensing, protein degradation, gene expression (Hart et al., 2007), and embryogenesis (Gambetta et al., 2009). UDP-GlcNAc and UDP-GalNAc are composed of four functional moieties as shown in Figure 1: glucose or galactose, ribose, acetyl, and UDP. These four functional moieties represent the convergence of several major metabolic pathways that lead from [U- ^{13}C]-glucose to UDP-GlcNAc and UDP-GalNAc biosynthesis as shown in Figure 2. These pathways include glycolysis, the citric acid cycle, the pentose phosphate pathway, pyrimidine biosynthesis, and the UDP-hexose biosynthetic pathway referred to as the "direct" pathway. Furthermore, other carbon sources can contribute to the synthesis of the uracil and acetyl moieties, to an extent that is cell and condition dependent. The moiety modeling seeks to determine the relative contributions for each pathway segment.

UDP-GlcNAc and UDP-GalNAc are handled together in this analysis because as these two metabolites have identical mass-to-charge ratios, the isotopologue peak intensities are the sum of both metabolites. However, from NMR isotopomer analysis (data not shown), UDP-GlcNAc is the major contributor to the isotopologue intensities and that this contribution is proportional across the set of isotopologue peaks. This makes logical sense because UDP-GlcNAc and UDP-GalNAc are separated by a single reversible enzymatic reaction catalyzed by the UDP-glucosamine epimerase.

2 METHODS

2.1 Data Acquisition and Natural Abundance Correction

LNCaP-LN3 prostate cancer cells (donated from Roswell Park) were grown to 70% confluence at 37º C in RPMI 1640 medium supplemented with: 10% FBS, 100 units/mL penicillin, 100 µg/mL streptomycin, 0.2% glucose, and 5% CO_2. Next, medium was replaced with a similar RPMI 1640 medium containing 0.2% [U-^{13}C] glucose. Cells were harvested at different time points, centrifuged, extracted with 10% trichloroacetic acid, lyophilized, and dissolved in H_2O. These samples were then analyzed via direct infusion nanoelectrospray FT-ICR-MS in negative ion mode using a Thermo 7T LTQ FT-MS. Isotopologue peaks were assigned using the software PREMISE (Lane et al., 2009) and each peak intensity was measured and normalized to the sum of the isotopologue intensities:

$$I_{n,obs} = I_{n,raw}/\Sigma\ I_{i,raw} \tag{1}$$

Finally, the set of UDP-GlcNAc and UDP-GalNAc isotopologue intensities were corrected for ^{13}C natural abundance using the following three equations implemented in an iterative algorithm (Moseley, 2010).

$$B_C(n,k) = \binom{C_{Max} - n}{k - n}(1 - NA_{13_C})^{C_{Max}-k}NA_{13_C}^{k-n} \tag{2}$$

$$B_C sum(n) = \sum_{k=n+1}^{C_{Max}} B_C(n,k) \tag{3}$$

$$I_{M+i} = \frac{I_{M+i;NA} - \sum_{x=0}^{x<i} I_{M+x} * B_C(x,i)}{1 - B_C sum(i)} \tag{4}$$

2.2 Moiety Modeling

As is shown in Figure 1, UDP-GlcNAc is composed of four functional moieties, glucose, ribose, acetyl, and uracil, representing convergence of several metabolic pathways. We can represent each moiety as a set of state variables reflecting the probabilities of ^{13}C incorporation into each moiety. The state variables **g0,r0,a0,u0** represent the probability of no ^{13}C incorporation in glucose, ribose, acetyl, and uracil, respectively. From Figure 2, it seems reasonable to restrict ^{13}C incorporation for glucose, ribose, and acetyl to the fully labelled state variables **g6**, **r5**, and **a2**, respectively. This is experimentally corroborated by the absence of partially labelled isotopomers of glucose, ribose, and acetate. Naturally, then the following relationships

hold for the state variables of glucose, ribose, and acetyl:

$$\mathbf{g6} = 1 - \mathbf{g0}$$
$$\mathbf{r5} = 1 - \mathbf{r0} \qquad (5)$$
$$\mathbf{a2} = 1 - \mathbf{a0}$$

However, the biosynthesis of uracil mixes ^{13}C from labelled glucose via $^{13}C_2$-acetyl-CoA with ^{12}C from other (unlabeled) sources during the citric acid cycle. Thus, multiple state variables $\mathbf{u1}, \mathbf{u2}$, and $\mathbf{u3}$ must be used to represent the partial labelling of uracil. There is no $\mathbf{u4}$ state variable since one carbon of uracil is derived from unlabeled CO_2. These state variables have the following relationship:

$$\mathbf{u0} + \mathbf{u1} + \mathbf{u2} + \mathbf{u3} = 1 \qquad (6)$$

The state variables for all four moieties can describe the probabilities for 32 different isotopomers of UDP-GlcNAc and the intensities for 18 isotopologues via the following set of equations:

$$I_0 = \mathbf{g0r0a0u0}$$
$$I_1 = \mathbf{g0r0a0u1}$$
$$I_2 = \mathbf{g0r0a0u2} + \mathbf{g0r0a2u0}$$
$$I_3 = \mathbf{g0r0a0u3} + \mathbf{g0r0a2u1}$$
$$I_4 = \mathbf{g0r0a2u2}$$
$$I_5 = \mathbf{g0r5a0u0} + \mathbf{g0r0a2u3}$$
$$I_6 = \mathbf{g6r0a0u0} + \mathbf{g0r5a0u1}$$
$$I_7 = \mathbf{g6r0a0u1} + \mathbf{g0r5a2u0} + \mathbf{g0r5a0u2}$$
$$I_8 = \mathbf{g6r0a2u0} + \mathbf{g6r0a0u2} + \mathbf{g0r5a0u3} + \mathbf{g0r5a2u1}$$
$$I_9 = \mathbf{g6r0a0u3} + \mathbf{g6r0a2u1} + \mathbf{g0r5a2u2} \qquad (7)$$
$$I_{10} = \mathbf{g6r0a2u2} + \mathbf{g0r5a2u3}$$
$$I_{11} = \mathbf{g6r5a0u0} + \mathbf{g6r0a2u3}$$
$$I_{12} = \mathbf{g6r5a0u1}$$
$$I_{13} = \mathbf{g6r5a0u2} + \mathbf{g6r5a2u0}$$
$$I_{14} = \mathbf{g6r5a0u3} + \mathbf{g6r5a2u1}$$
$$I_{15} = \mathbf{g6r5a2u2}$$
$$I_{16} = \mathbf{g6r5a2u3}$$
$$I_{17} = \text{NA contribution only}$$

In addition, these state variables and their constraining relationships provide six optimizable parameters ($\mathbf{g6}$, $\mathbf{r5}$, $\mathbf{a2}$, $\mathbf{u1}$, $\mathbf{u2}$, $\mathbf{u3}$), one each for glucose, ribose, and acetyl and three for uracil. These variables are time dependent, and constitute the starting point for detailed flux analysis of the

specific metabolic network that described the synthesis of the observed product.

2.3 GAIMS

To extract the variables from the data, we have developed a combined simulated annealing and genetic algorithm called Genetic Algorithm for Isotopologues in Metabolic Systems (GAIMS) to optimize moiety model parameters. GAIMS uses a description of the moiety model to calculate isotopologue intensities (Equations 7). The program then uses these calculated isotopologue intensities ($I_{n,calc}$) with the observed experimental isotopologue intensities ($I_{n,obs}$) to create a target function that compares calculated isotopologue intensities to their experimentally observed counterparts:

$$\text{target\_function} = \Sigma \text{abs}(I_{n,obs} - I_{n,calc}) \qquad (8)$$

Other target functions were tested including the commonly used sum of squared differences; however, that function tended to fit stronger isotopologue intensities at the expense of weaker isotopologue intensities. Also, target functions normalized by intensity demonstrated poorer convergence, probably due to the higher fractional error in the weaker isotopologue intensities. Overall, the target function represented by Equation 8 provided the best behaviour.

For each parameter optimization, GAIMS used a linear annealing scheme over 1,000,000 steps. Genetic algorithm settings included a population size of 20 with a cross-over versus mutation rate ratio of 1:20. Mutation steps changed three parameters at a time to compensate for any dependencies between parameters. Each optimization was performed 50 times to verify robustness (i.e. avoidance of local minima) and to provide meaningful statistics of convergence.

2.4 Model Selection using AIC

We developed a model selection method using the following form of the Akaike information criterion or AIC (Akaike, 1974):

$$AIC \approx 2k + n \log\left(\frac{\Sigma_{i=1}^{n}\left(I_{i,obs} - I_{i,calc}\right)^2}{n}\right) \qquad (9)$$

In Equation 9, k is the number of moiety model parameters being optimized. The log of the average sum of squares of differences approximates the log likelihood of a given model. The calculated

isotopologue intensities $I_{i,calc}$ are derived from average moiety model parameters for all 50 optimizations. With this equation, we can compare models with a different number of optimizable parameters. This model selection method was developed as a part of GAIMS.

3 RESULTS

3.1 Fit of Expert-Derived Moiety Model

Figure 3 shows the fit of calculated isotopologue intensities from the expert-derived moiety model (Equations 7) to the 72-hour time point of experimental isotopologue intensities representing both UDP-GlcNAc and UDP-GalNAc. From this fit, we obtain values for each functional moiety state variable. All fifty optimizations converged quite well as indicated by the standard deviations in state variables. Interestingly, the fit of high intensity isotopologues appears better than low intensity isotopologues. In addition, we repeated this analysis with 50 optimizations using 10,000,000 steps and 50 optimizations using 100,000 steps and obtained very similar results in both parameter values and standard deviations (data not shown), further demonstrating the robustness of the parameter optimization.
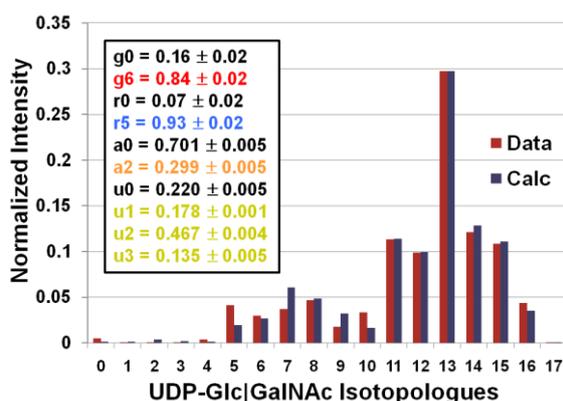

Figure 3: Fit of optimized expert-derived moiety model to FT-ICR-MS isotopologue data of UDP-GlcNAc and UDP-GalNAc from tissue culture sample after 72 hours of labeling with uniformly ^{13}C-labeled glucose.

3.2 Comparison of Models Using a Target Function

To explore reasons why some of the low intensity isotopologues did not fit as well, we examined alternative moiety models that tested assumptions of

our original model. From the pathway diagram in Figure 2, there is the possibility that scrambling of ^{13}C incorporation in the acetyl moiety might be occurring via amino acid biosynthetic and catabolic pathways on the time-scale of 72 hours. So we created an extended acetyl model with additional terms (i.e., $I_1 = g0r0a0u1 + g0r0a1u0$) in Equations 7 using the acetyl moiety state variable $a1$ along with the following relationship:

$$a0 + a1 + a2 = 1 \qquad (10)$$

In a similar manner, we created another alternative moiety model with the addition of the $u4$ state variable for the uracil moiety. This CO_2-inclusive model tested the hypothesis that all CO_2 used in uracil biosynthesis is unlabeled. Likewise, the relationship between uracil state variables was expanded in the following manner:

$$u0 + u1 + u2 + u3 + u4 = 1 \qquad (11)$$

Table 1 shows the comparison between the three moiety models. The value indicated for the target function is the average across all 50 optimizations for each model. Equation 8 clearly indicates that this is a minimizing target function and thus lower values are better.

Table 1: Comparison between three moiety models using the average value of the target function.

CO₂-Inclusive (7_G1R1A1U4)	Expert-Derived (6_G1R1A1U3)	Extended Acetyl (7_G1R1A2U3)
TF = 0.1103	TF = 0.1096	TF = 0.0913
g0 = 0.15	g0 = 0.16	g0 = 0.15
g6 = 0.85	g6 = 0.84	g6 = 0.85
r0 = 0.08	r0 = 0.07	r0 = 0.08
r5 = 0.92	r5 = 0.93	r5 = 0.92
a0 = 0.70	a0 = 0.70	a0 = 0.28
a2 = 0.30	a2 = 0.30	a1 = 0.15
u0 = 0.22	u0 = 0.22	a2 = 0.57
u1 = 0.18	u1 = 0.18	u0 = 0.54
u2 = 0.47	u2 = 0.47	u1 = 0.15
u3 = 0.14	u3 = 0.14	u2 = 0.22
u4 = 0.001		u3 = 0.09

The results in Table 1 clearly indicate that the CO_2-inclusive model is worse than the expert-derived model. Moreover, the extended acetyl model appears to be the best model. However, the extended acetyl model has one additional optimizable parameter, which might afford the improvements observed in the target function.

We also optimized an additional CO_2-inclusive model where the ^{13}C incorporation via CO_2 was modelled as its own state variables $c0$ and $c1$. This

moiety model gave very similar results to those for the original CO_2-inclusive model, indicating that the specific implementation of a model is not critical (data not shown).

3.3 Comparison of Models Using AIC

We used the form of the AIC in Equation 9 to address the issue of model comparison involving different number of optimizable parameters. The AIC is calculated for each model using the average parameter values across the 50 GAIMS optimizations. But instead of just comparing three possible models, we created a set of over 40 moiety models to compare, ranging from plausible to completely nonsense models. The expert-derived model is represented by the identifier 6_G1R1A1U3, where the first number indicates the number of optimizable parameters in the model and G1R1A1U3 represents one parameter in the glucose moiety, one parameter in the ribose moiety, one parameter in the acetyl moiety, and three parameters in the uracil moiety, respectively. Deviations from the expert-derived model are indicated by state variables that are modified or added.

Table 2: Comparison of 40 moiety models using the AIC and the experimental FT-ICR-MS isotopologue data of UDP-GlcNAc and UDP-GalNAc at the 72-hour time point.

AIC	Moiety Model
-157.43	**6_G0R2A1U3_g3r2r3_g6r5**
-109.64	6_G1R1A1U3_a1
-136.29	6_G1R1A1U3_g5
-154.32	6_G1R1A1U3
-137.17	6_G1R1A1U3_r4
-133.12	6_G1R1A1U3_u4
-159.00	**7_G0R2A2U3_g3r2r3_g6r5**
-72.52	7_G0R3A1U3_g3r2r3_g6r5_g5r4
-72.52	7_G0R3A1U3_g3r2r3_g6r5_r4
-151.40	7_G1R1A1U3C1
-153.52	7_G1R1A1U4
-156.29	**7_G1R1A2U3**
-158.25	**7_G1R2A1U3_g3r2r3**
-153.65	7_G1R2A1U3_r1
-159.24	**7_G1R2A1U3_r2**
-147.55	7_G1R2A1U3_r3
-163.39	**7_G1R2A1U3_r4**
-153.95	7_G2R1A1U3_g1
-153.64	7_G2R1A1U3_g2
-158.87	**7_G2R1A1U3_g3**
-151.21	7_G2R1A1U3_g4
-160.84	**7_G2R1A1U3_g5**
-154.17	8_G1R1A2U3C1
-156.58	**8_G1R2A2U3_g3r2r3_g6r5_g5**
-158.22	**8_G1R2A2U3_g3r2r3**
-154.14	8_G1R2A2U3_r1
-159.10	**8_G1R2A2U3_r2**
-157.39	**8_G1R2A2U3_r2r3**
-148.47	8_G1R2A2U3_r3
-161.97	**8_G1R2A2U3_r4**
-153.91	8_G2R1A2U3_g1
-154.09	8_G2R1A2U3_g2
-158.85	**8_G2R1A2U3_g3**
-151.36	8_G2R1A2U3_g4
-159.52	**8_G2R1A2U3_g5**
-155.89	**9_G2R2A2U3_r2r3_g1**
-154.77	**9_G2R2A2U3_r2r3_g2**
-156.24	**9_G2R2A2U3_r2r3_g3**
-152.79	9_G2R2A2U3_r2r3_g4
-156.13	**9_G2R2A2U3_r2r3_g5**
-155.50	**9_G2R2A2U3_r2r3_g6r5_g3_g5**

Table 2 shows the AIC for all these models based on the 72-hour time point of experimental isotopologue intensities. The models in red all indicate AICs that are better than the expert-derived model. However, the 7_G1R2A1U3_r4 model gave the best (lowest) AIC even though this model with ribose state variables **r5**, **r4**, and **r0** makes no biochemical sense given the known information about the pentose phosphate pathway in human cells. In fact, many nonsense models gave better results than the expert-derived model, indicating a significant problem with overfitting.

3.4 Model Selection Using AIC with Multiple Time Points

Table 3: Comparison of 40 moiety models using the AIC and the experimental FT-ICR-MS isotopologue data of UDP-GlcNAc and UDP-GalNAc at the 34-hour, 48-hour, and 72-hour time points.

AIC	Moiety Model
-321.81	6_G0R2A1U3_g3r2r3_g6r5
-355.87	6_G1R1A1U3_a1
-326.98	6_G1R1A1U3_g5
-428.98	**6_G1R1A1U3**
-332.69	6_G1R1A1U3_r4
-308.16	6_G1R1A1U3_u4
-291.31	7_G0R2A2U3_g3r2r3_g6r5
-287.32	7_G0R3A1U3_g3r2r3_g6r5_g5r4
-290.16	7_G0R3A1U3_g3r2r3_g6r5_r4
-306.58	7_G1R1A1U3C1
-293.12	7_G1R1A1U4
-299.86	7_G1R1A2U3
-294.52	7_G1R2A1U3_g3r2r3
-308.59	7_G1R2A1U3_r1
-288.94	7_G1R2A1U3_r2
-277.44	7_G1R2A1U3_r3
-244.47	7_G1R2A1U3_r4
-318.01	7_G2R1A1U3_g1
-317.89	7_G2R1A1U3_g2
-286.93	7_G2R1A1U3_g3
-277.12	7_G2R1A1U3_g4

-252.21	7_G2R1A1U3_g5
-288.84	8_G1R1A2U3C1
-296.01	8_G1R2A2U3_g3r2r3_g6r5_g5
-288.88	8_G1R2A2U3_g3r2r3
-290.93	8_G1R2A2U3_r1
-296.67	8_G1R2A2U3_r2
-296.18	8_G1R2A2U3_r2r3
-251.87	8_G1R2A2U3_r3
-239.25	8_G1R2A2U3_r4
-303.97	8_G2R1A2U3_g1
-293.45	8_G2R1A2U3_g2
-288.32	8_G2R1A2U3_g3
-260.59	8_G2R1A2U3_g4
-236.42	8_G2R1A2U3_g5
-293.74	9_G2R2A2U3_r2r3_g1
-279.33	9_G2R2A2U3_r2r3_g2
-291.46	9_G2R2A2U3_r2r3_g3
-241.63	9_G2R2A2U3_r2r3_g4
-227.58	9_G2R2A2U3_r2r3_g5
-276.84	9_G2R2A2U3_r2r3_g6r5_g3_g5

To address the issue of overfitting, we optimized the isotopologue data for the 34-hour, 48-hour, and 72-hour time points simultaneously and calculated an AIC for the combined optimization. The expert-derived model had the best AIC of -428.98. The next best model 6_G1R1A1U3_a1 was significantly worse with an AIC of -355.87, indicating that overall, the expert-derived model provides the best description of the data.

4   CONCLUSIONS

We have demonstrated a novel metabolic modelling methodology applied to FT-ICR-MS isotopologue intensity data for UDP-GlcNAc and UDP-GalNAc. Our implementation, GAIMS, interprets a set of isotopologues as the flow of functional moieties through metabolic pathways. This is represented by a set of optimizable parameters for a given moiety model. Figure 2 demonstrates a solid convergence of 50 individual optimizations for an expert-derived model based on what is currently known about UDP-GlcNAc biosynthesis. However, the standard deviations for parameter values should not be interpreted as a close representation of parameter error, especially with the indication of model overfitting in results from Table 2.

In addition, we demonstrate a robust model selection method, which uses a form of the Akaike information criterion (Equation 9). Our use of the average parameter values from a set of optimizations allows the AIC to sense smoothness of the error surface for the target function of a given moiety

model. This application of the AIC along with the use of isotopologues from multiple time points enables our model selection method to overcome issues of model overfitting for a set of isotopologues at individual time points. We envision the coupling of this robust model selection method with newer non-steady-state metabolic flux analytical methods (Selivanov et al., 2006; Wahl et al., 2008) as a logical next step.

ACKNOWLEDGEMENTS

REFERENCES

Akaike, H., 1974. "A new look at the statistical model identification", *IEEE Transactions on Automatic Control,* 19, 716–723.

Edwards, J.S., Ibarra, R.U., Palsson, B.O., 2001. "In silico predictions of *Escherichia coli* metabolic capabilities are consistent with experimental data", *Nature Biotech*, 19, 125-130.

Fell, D.A., 1984. "Fat synthesis in adipose tissue. An examination of stoichiometric constraints", *J Biochem*, 238, 781-786.

Fell, D.A., 1997. *Understanding the Control of Metabolism*, London: Portland Press.

Gambetta, M.C., Oktaba, K., & Müller, J., 2009. "Essential Role of the Glycosyltransferase Sxc/Ogt in Polycomb Repression", *Science,* 325, 93-96.

Harrigan, G.G., Goodacre, R. (Ed), 2003. *Metabolic profiling: its role in biomarker discovery and gene function analysis*, Boston: Kluwer Academic Publishers.

Hart G.W., Housley M.P., Slawson C., 2007. "Cycling of O-linked beta-N-acetylglucosamine on nucleocytoplasmic proteins", *Nature,* 446, 1017-1022.

Hellerstein, M.K., 2003. "In vivo measurement of fluxes through metabolic pathways: the missing link in functional genomics and pharmaceutical research", *Annu Rev Nutr*, 23, 379-402.

Kauffman, K.J., Prakash, P., Edwards, J.S., 2003. "Advances in flux balance analysis", *Curr Opin Biotech*, 14, 491-496.

Lane A.N., Fan T.W-M., Higashi R.M., 2008. "Isotopomer-based metabolomic analysis by NMR and mass spectrometry". *Methods in Cell Biology*,Vol 84. Biophysical Tools for Biologists, Vol 1,ed. Correia JJ, Detrich HW. Elsevier Science & Technology Books Ch.18. 541-588.

Lane, A.N., Fan, T.W-M., Xie, Z., Moseley, H.N.B., Higashi, R.M., 2009. "Stable isotope analysis of lipid biosynthesis by high resolution mass spectrometry and NMR.", *Anal Chim Acta*, 651, 201-208.

Moseley, H.N.B., 2010. "Correcting for the Effects of Natural Abundance in Stable Isotope Resolved Metabolomics Experiments Involving Ultra-High Resolution Mass Spectrometry", *BMC Bioinformatics*, 11, 139-144.

Savinell, J.M., Palsson, B.O., "Optimal selection of metabolic fluxes for in vivo measurement. I. Development of mathematical methods", *J Theor Biol*, 155, 201-214.

Sauer, U., Lasko, D.R., Fiaux, J., Hochuli, M., Glaser, R., Szyperski, T., Wuthrich, K., Bailey, J.E., 1999. "Metabolic Flux Ratio Analysis of Genetic and Environmental Modulations of Escherichia coli Central Carbon Metabolism", *J Bacteriol*, 181, 6679-6688.

Sauer, U., 2006. "Metabolic networks in motion: 13C-based flux analysis", *Mol Syst Biol*, 2, 62.

Schellenberger, J., Palsson, B.O., 2009. "Use of Randomized Sampling for Analysis of Metabolic Networks", *J Biol Chem*, 284, 5457-5461.

Selivanov, V.A., Marin, S., Lee, P.W.N., Cascante, M., 2006. "Software for dynamic analysis of tracer-based metabolomics data: estimation of metabolic fluxes and their statistical analysis", *Bioinformatics*, 22, 2806-2812.

Stephanopoulos, G., "Metabolic fluxes and metabolic engineering", *Metab Eng*, 1, 1-11.

Wahl, S.A., Nöh, K., Wiechert, W., 2008. "13C labelling experiments at metabolic nonstationary conditions: An exploratory study", *BMC Bioinformatics*, 9, 152-169.